RESEARCH ARTICLE

Epigenetic Dynamics of Imprinted X Inactivation During Early Mouse Development

Ikuhiro Okamoto,[1] Arie P. Otte,[2] C. David Allis,[3] Danny Reinberg,[4] Edith Heard[1]*

The initiation of X-chromosome inactivation is thought to be tightly correlated with early differentiation events during mouse development. Here, we show that although initially active, the paternal X chromosome undergoes imprinted inactivation from the cleavage stages, well before cellular differentiation. A reversal of the inactive state, with a loss of epigenetic marks such as histone modifications and polycomb proteins, subsequently occurs in cells of the inner cell mass (ICM), which give rise to the embryo-proper in which random X inactivation is known to occur. This reveals the remarkable plasticity of the X-inactivation process during preimplantation development and underlines the importance of the ICM in global reprogramming of epigenetic marks in the early embryo.

In mammals, dosage compensation between XX females and XY males is achieved by inactivating one of the two X chromosomes during early female embryogenesis (*1*). Classical biochemical and cytological analyses have suggested that in XX mouse embryos, there are three waves of X inactivation during development, correlating with the three earliest differentiation steps (*2*). In the first two lineages to differentiate, the trophectoderm and primitive endoderm of the blastocyst, which contribute to the extraembryonic tissues, X inactivation is subject to imprinting, with exclusive inactivation of the paternal X chromosome (Xp) (*3*, *4*). This seems to be due to an imprint on the maternal X chromosome (Xm) to remain active, as well as a paternal imprint to inactivate (*5*). By the third wave of differentiation, in epiblast cells derived from the ICM, X inactivation is random, affecting either the Xp or the Xm (*6*, *7*). Initiation of both imprinted and random X inactivation are dependent on a unique, untranslated RNA (Xist) that coats the X chromosome in cis and triggers its silencing (*8*, *9*). In embryonic stem (ES) cells, which can recapitulate the random form of X inactivation upon in vitro differentiation, Xist RNA coating of the X chromosome is rapidly followed (within one to two cell cycles) by gene silencing (*10*). During early development, *Xist* is expressed from the two- to four-cell stage onward (*11*–*13*). Early *Xist* expression is exclusively of paternal origin (*11*); the maternal *Xist* allele is repressed until the morula stage (*12*). Despite the early Xist RNA coating of the Xp at the four-cell stage (*12*), the first cytologically detectable signs of X inactivation (a heteropycnotic, asynchronously replicating Xp) occur several cell divisions later, at about the 50-cell stage in the trophectoderm (*14*, *15*). The reasons for this apparent delay, which contrasts with the rapidity of X inactivation that occurs after Xist RNA coating in differentiating ES cells, remain unclear. Furthermore, even though both the Xm and Xp are clearly active immediately after fertilization based on allozyme analysis (*16*–*18*), reverse transcription polymerase chain reaction (RT-PCR) studies have suggested that paternal alleles of some X-linked genes show lower transcriptional activity than their maternal counterparts during early embryogenesis (*19*, *20*). Indeed, it has been suggested that a predisposition of the XP to inactivate may be carried over from its passage through the male germ line, where the Xp and the Y chromosome together form the highly condensed, heterochromatic sex vesicle, and this could underly imprinted X inactivation (*21*).

Xist RNA and early chromatin changes on Xp. A number of unresolved questions thus surround the initiation and kinetics of imprinted X inactivation. We set out to address these questions with techniques that enable us to examine the status of the Xist RNA–coated Xp in individual cells during early preimplantation embryogenesis. Embryos from the two-cell to the blastocyst stage were isolated by flushing from the oviduct or uterus and analyzed directly, without in vitro culture, which can potentially lead to perturbations in epigenetic regulation. Using RNA fluorescence in situ hybridization (FISH), a domain of Xist RNA accumulation could be detected in all interphase blastomeres from the four-cell stage onward (Figs. 1 and 2 and fig. S1). These findings are consistent with previous studies (*12*, *13*, *22*, *23*). We could detect a small punctate signal but no Xist RNA accumulation in a proportion of two-cell embryos (in the G_2 phase based on developmental timing). At the four-cell stage, when paternal Xist RNA is just starting to accumulate, the Xist RNA domain was often small (Fig. 2 and fig. S3). We examined the early chromatin status of the Xp chromosome by means of Xist RNA FISH combined with immunofluorescence. In particular, we looked for Xp enrichment in H3 histones methylated at lysines 9 (K9) and 27 (K27) and for its association with the Eed and Enx1 polycomb group proteins (see table S1 for antibodies), because all of these marks have been shown to be characteristics of the X chromosome undergoing inactivation, and therefore represent candidates for the predisposition of the Xp to inactivate (*24*–*27*). Methylation of H3K9, in particular, has been reported to be associated with the Xp in the sex vesicle during spermatogenesis (*28*). When we examined four- and eight-cell stage embryos, no sign of either H3K9 and H3K27 methylation enrichment or of Eed and Enx1 accumulation could be detected on the Xist RNA–coated Xp (Fig. 1). At the 16-cell stage, however, these marks could be detected on the Xp in some blastomeres (Fig. 1 and fig. S2). Their similar time of onset on the Xp is consistent with Enx1 being the histone methyltransferase responsible for H3K27 methylation (*26*, *27*). This is also the time window previously described for accumulation of the histone H2A variant, macroH2A, on the X chromosome (*29*), suggesting that major chromatin changes on the Xp begin at this stage. The proportion of blastomeres in which the Xp carried the Eed, Enx1, and H3K27 methylation marks varied considerably between embryos at the 16- to 32-cell stages (Fig. 1, i and r). By the blastocyst stage, however, the Xp carried these marks in the majority (>90%) of blastomeres. Methylation of H3K9 on the Xp showed different kinetics, with a later onset, which were first detected in embryos with >32 cells (Fig. 1 and fig. S2). By the midblastocyst stage, almost all trophectoderm cells had an Xp enriched in H3K9 methylation (Fig. 1, p and q). The later appearance of H3K9 methylation on the Xp suggests that this mark may be independently deposited, perhaps as a consequence of H3K27 methylation.

We also examined the timing of X-chromosome–wide hypoacetylation of H3K9 and hypomethylation of H3K4. These are early events

[1]CNRS UMR218, Curie Institute, 26 rue d'Ulm, Paris 75005, France. [2]Swammerdam Institute for Life Sciences, BioCentrum Amsterdam, University of Amsterdam, 1018 TV Amsterdam, Netherlands. [3]Rockefeller University, Box 78, 1230 York Avenue, New York, NY 10021, USA. [4]Department of Biochemistry, Division of Nucleic Acids Enzymology, Howard Hughes Medical Institute, University of Medicine and Dentistry of New Jersey, Robert Wood Johnson Medical School, Piscataway, NJ 08854, USA.

*To whom correspondence should be addressed. E-mail: edith.heard@curie.fr

during random X inactivation in differentiating ES cells; they occur within the same time window as H3K9 and K27 methylation (*24*, *26*, *30*). At the four-cell stage, no or very little depletion for these histone modifications could be detected at the site of Xist RNA accumulation (Fig. 2, a to d, and fig. S3A). However, at the 8-cell stage, both hypoacetylation of H3K9 and hypomethylation of H3K4 could be detected at the Xp in some blastomeres (Fig. 2, c to f), and by the 32-cell stage, the proportion of blastomeres with an Xp carrying these marks had risen to over 90% (Fig. 2i). Thus, hypoacetylation of H3K9 and hypomethylation of H3K4 occur after Xist RNA coating of the Xp chromosome, but precede Eed/Enx1 accumulation and H3K27 and K9 methylation.

Transcriptional activity of the Xp. The surprisingly early appearance of these chromatin changes on the Xp suggested that the initiation of Xp inactivation could be more precocious than previously thought. Studies on the developmental timing of Xp inactivation have, in the past, involved analysis at the posttranscriptional level (RT-PCR) (*19*, *20*) or posttranslational level [allozyme analyses, LacZ,

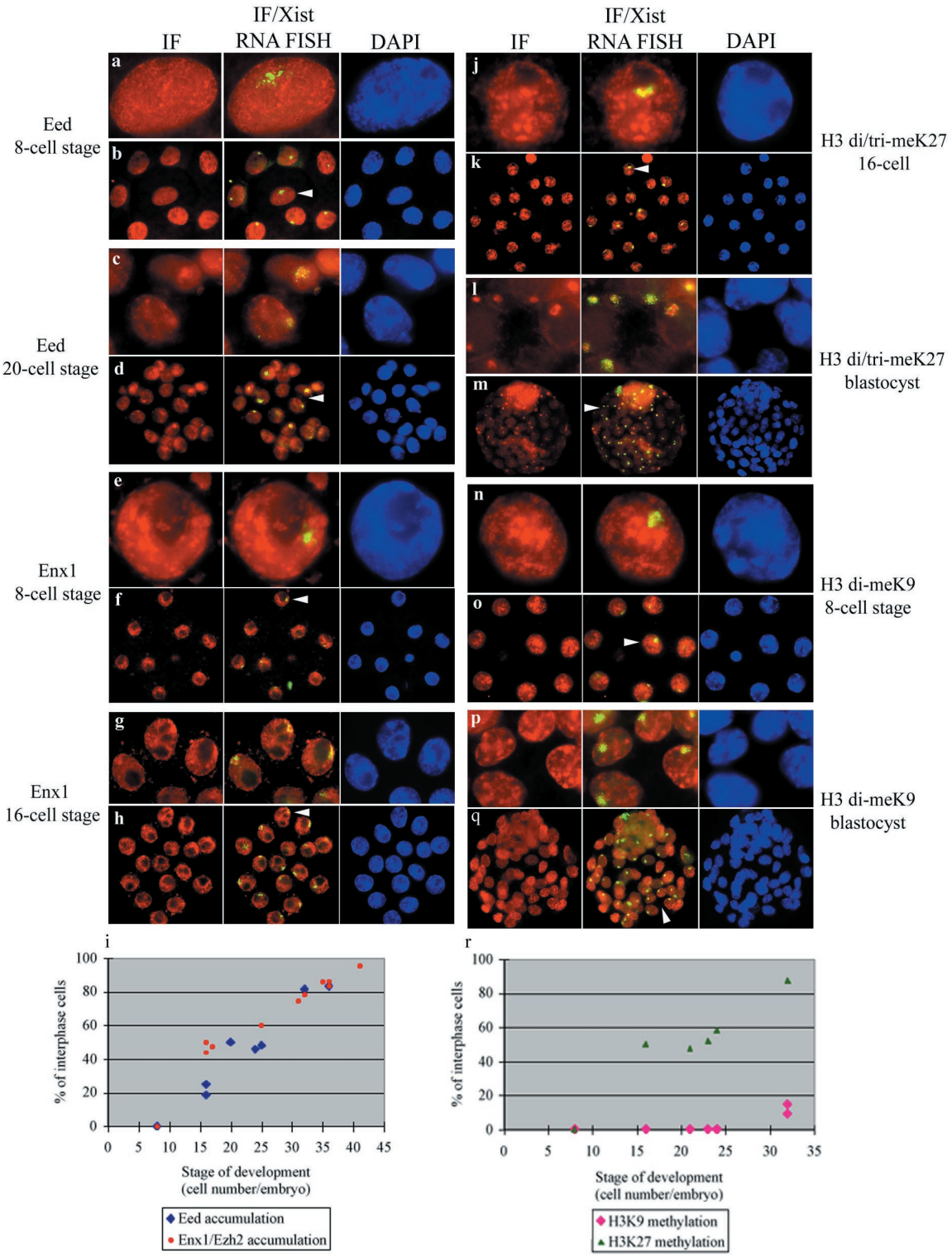

Fig. 1. Eed, Enx1, and histone H3 methylation enrichment on the Xp in preimplantation embryos. Immunolabeling (red) with antibodies against Eed (**a** to **d**), Enx1 (**e** to **h**), H3 di/trimethyl K27 (**j** to **m**), and H3 dimethyl K9 (**n** to **q**) was combined with Xist RNA FISH (green). 4′,6′-diamidino-2-phenylindole (DAPI) staining is shown in blue. For each stage, an intact embryo and enlarged representative nucleus or nuclei are shown. The arrowheads indicate which cells are shown enlarged above each embryo. The number of embryos with blastomeres showing Xp enrichment of Eed and Enx1 (**i**) or H3K27 and H3K9 methylation (**r**) are shown.

and green fluorescent proteins (GFPs)] (*4*, *31*, *32*) and were hampered by the use of pools of embryos or cells, as well as the unknown half-lives of the X-linked transcripts and proteins assayed. We therefore decided to assess Xp silencing more directly, at the level of transcription and in single cells. Using an antibody (H5) that recognizes the elongating form of RNA polymerase II (RNA PolII), which is normally present only in transcriptionally engaged chromatin (*33*), we assessed the presence or absence of RNA PolII from the Xist RNA domain as a marker of transcriptional activity or silencing of the Xp. In differentiating female ES cells, we found that RNA PolII exclusion from the X

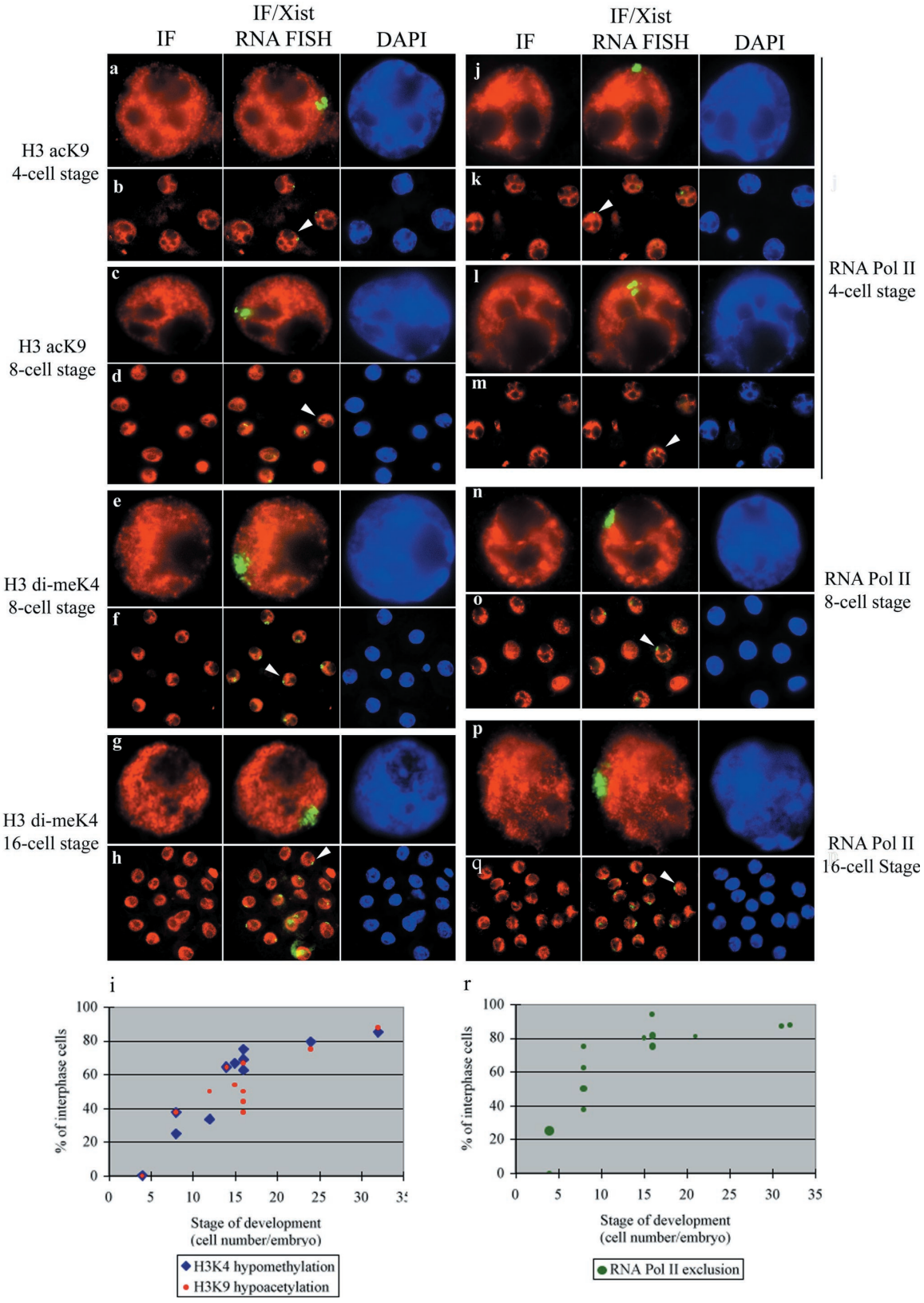

Fig. 2. Loss of histone H3K4 methylation, H3K9 acetylation, and RNA PolII from the Xp in early preimplantation embryos. Immunolabeling (red) with antibodies was combined with Xist RNA FISH (green). 4′,6′-diamidino-2-phenylindole (DAPI) staining is shown in blue. Hypoacetylation of H3K9 (**a** to **d**) and hypomethylation of H3K4 (**e** to **h**) are seen in some blastomeres from the eight-cell stage. Two focal planes of the same four-cell embryo are shown illustrating the initiation of RNA PolII exclusion (detected with antibody H5) in some blastomeres (**j** and **k**) but not in others (**l** and **m**). Eight-cell and sixteen-cell embryos show complete RNA PolII exclusion from the Xp in most blastomeres (**n** to **q**). Arrowheads indicate which cells of the intact embryo are shown as an enlarged version. Kinetics of these changes on the Xp are shown in (**i**) and (**r**).

chromosome is one of the earliest events in the X-inactivation process, after Xist RNA coating (*34*). Using this approach in preimplantation embryos, we could see no exclusion of RNA PolII at or around the location of the Xist pinpoint signal detected in two-cell, G_2 stage embryos (fig. S3). The first signs of exclusion of RNA PolII from the site of Xist RNA accumulation on the Xp could be detected at the four-cell stage (Fig. 2, j to m). The number of blastomeres showing this pattern increased from one or two at the 4-cell stage to almost 100% by the 32-cell stage (Fig. 2r and fig. S3, i to l). The early initiation of transcriptional silencing of the Xp was confirmed with RNA FISH to detect nascent transcripts of the X-linked Chic1/Brx gene. At the two-cell stage, two Chic1/Brx signals, one of which was adjacent to the *Xist* pinpoint, could be seen in some embryos (fig. S3). At the 8-cell stage a *Chic1/Brx* RNA signal could be detected on the Xp within the Xist RNA domain in some blastomeres, but by the 16-cell stage, this pattern was never seen in more than one blastomere (*35*). Taken together, our data point to the initiation of transcriptional inactivation of the Xp from the four- to eight-cell stage, which is much earlier than previously thought. Before this, at the two-cell stage, the Xp seems to be active. Inactivation appears to be triggered by Xist RNA coating of the Xp and affects most if not all blastomeres by the 32-cell stage. Imprinted X inactivation thus initiates before any overt signs of cellular differentiation.

Inactivation status of the Xp in the ICM. By the late morula/early blastocyst stage (the first sign of the blastocoel cavity), our findings suggest that essentially all blastomeres contain an inactive Xp, as assessed by RNA

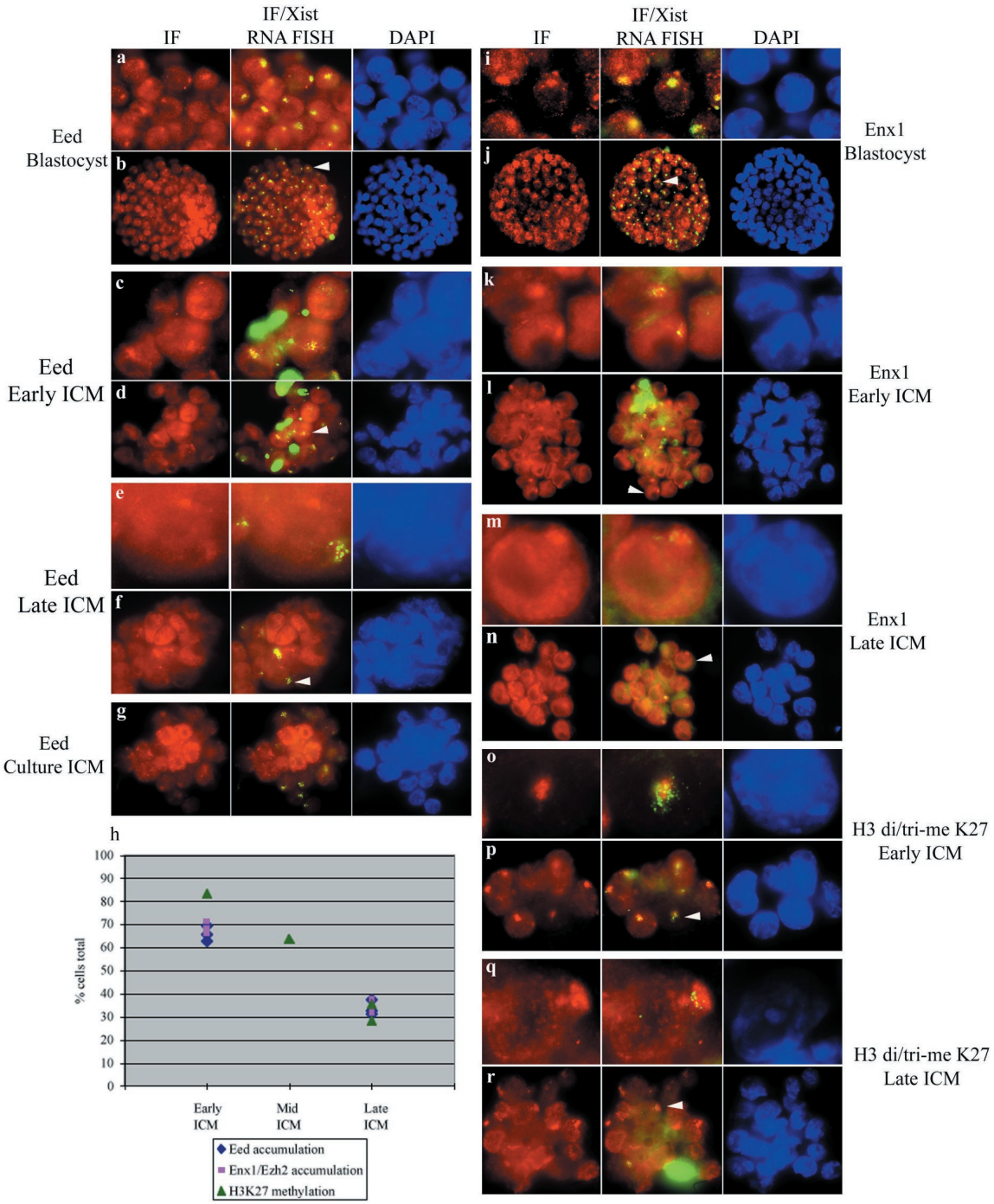

Fig. 3. Blastocysts and ICM cells isolated at different stages with immunosurgery (*42*) are shown. Eed, Enx1, or H3 di/tri-meK27 was detected by immunolabeling (red) combined with Xist RNA FISH. 4′,6′-diamidino-2-phenylindole (DAPI) staining is shown in blue. Representative trophectoderm cells (arrowheads) with Eed (**a** and **b**) and Enx1 (**i** and **j**) accumulation on the Xist RNA–coated chromosome are shown. Eed staining and Xist RNA FISH in ICM cells derived from early, late, and cultured blastocysts is shown (**c** to **g**). Xist RNA FISH and Enxl staining (**k** to **n**) or H3 di/trimethyl K27 staining (**o** to **r**) in ICM cells derived from early and late blastocysts are shown. The decreasing proportions of cells showing Eed, Enx1, or H3 di/tri-meK27 enrichment in the ICM are summarized (**h**).

PolII exclusion, histone modifications, and Eed/Enx1 association. An important implication of this is that the Xp must be inactive even in the ICM, which gives rise to the epiblast. However, it is well known that random and not imprinted paternal inactivation occurs in this lineage. To resolve this paradox, we investigated the activity status of the Xp specifically in the ICM, using immunosurgery to isolate ICMs and eliminate all trophectoderm cells. When this procedure was performed on early blastocysts, the isolated ICM cells were found to contain a Xist RNA domain from which RNA PolII staining was excluded (fig. S4, e and f) and which was associated with H3K9 hypoacetylation, H3K4 hypomethylation, H3K9 and K27 methylation, and Eed and Enx1 accumulation (Fig. 3, k to n) (*35*). Thus, exactly as predicted by our kinetic analysis, the Xist RNA–coated Xp appears to be inactive in all cells, including those of the ICM, up to the early blastocyst stage. However, when ICM immunosurgery was performed on later (expanded or hatching) blastocysts, we found that, in contrast to trophectoderm cells, in the majority of ICM cells, Xist RNA appeared to be dispersed or absent and no Eed- or Enx-enriched domain could be found. Thus, during ICM growth, Xist RNA coating of the Xp is lost, and this is tightly coupled to loss of Eed and Enx1 accumulation on the Xp (Fig. 3h). However, the majority of these cells still contained what appeared to be an X-chromosome domain enriched in H3K27 methylation, even in the absence of Xist RNA coating. In ICMs from the latest blastocysts recovered, some cells had also lost the H3K9 and K27 methylation domain, even though these modifications could clearly be detected elsewhere in the nucleus (Fig. 3, q and r). Histone H3K9 and K27 methylation are therefore also lost on the Xp over time in the ICM, but after the dissociation of Xist RNA, Eed, and Enx1 (Fig. 4a).

We also isolated the ICM from early blastocysts by immunosurgery and cultured them for 24 hours. In this procedure, the outgrowing cells are believed to be of the primitive endoderm type (*15*, *36*). All outgrowing cells were found to have a Xist RNA domain that showed the chromatin characteristics observed in morulas and in the trophectoderm (Fig. 3g) (*35*), suggesting that the inactive state of the Xp is probably maintained upon differentiation of the primitive endoderm lineage. On the other hand, in cells at the center of the ICM, reversal of the inactive state (loss of Xist RNA coating, as well as loss of Eed and Enx association) could be detected, as in ICMs isolated directly from late blastocysts.

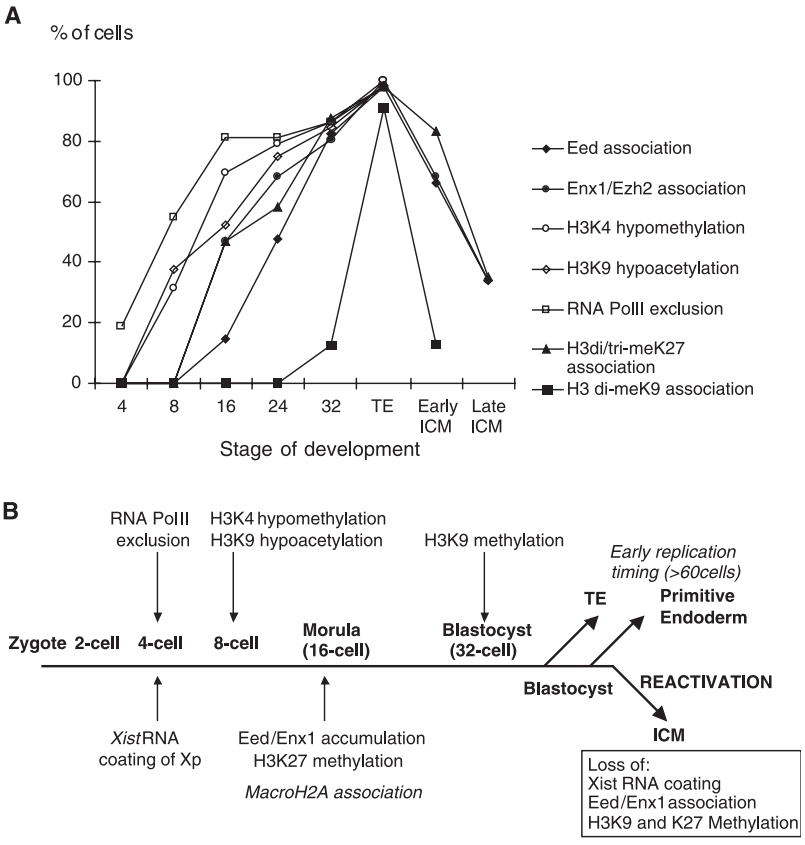

Fig. 4. The kinetics of transcriptional inactivation, histone modifications, and polycomb group protein association on the Xist RNA–coated Xp in preimplantation embryos are summarized (**A**), and a schematic representation of the order events is shown (**B**). Findings not shown here but reported by others (*13*, *14*, *28*) are shown in italics.

Conclusions. We have made a number of findings concerning the process of X inactivation during early mouse development. We show that the imprint on the Xp is unlikely to be due to its global chromatin status but rather to the early activity of the paternal *Xist* gene. We also show that, although the Xp is initially active in early cleavage female embryos, it becomes rapidly inactivated after accumulation of Xist RNA at the four-cell stage, as assessed by the exclusion of RNA PolII, the absence of nascent X-linked transcripts, and the appearance of H3K4 hypomethylation and H3K9 hypoacetylation. Polycomb group proteins, which are believed to be involved in the early maintenance of the repressed state in several systems (*37*) and X inactivation in particular (*26*, *27*), subsequently accumulate on the Xp and H3K27 methylation occurs. The variable time of onset we observed for these early maintenance marks over the 16- to 32-cell stage may explain the potential reversibility of Xp imprinted inactivation in some embryos, under abnormal circumstances such as in XpO (with no Xm and a single Xp) mice (*38*) or in androgenotes (XpXp) (*22*). From the 32-cell stage onward, however, we show that the Xp carries these epigenetic marks in virtually all cells of female embryos and maintains them in the trophectoderm and primitive endoderm. In these lineages, they are presumably further "locked in" by the shift in replication timing of the Xp (*14*). However, during ICM growth, we found that X inactivation is reversed. A rapid loss of Xist RNA coating of the Xp was observed, accompanied by the loss of Eed and Enx1 association, and this was followed by a more gradual loss of the H3 methylation marks, presumably by dilution of old nucleosomes through cell division. By the time implantation occurs, the Xp is no longer inactive and random inactivation of either the Xp or the Xm can occur in cells of the epiblast. The kinetics of these events are shown in Fig. 4a, together with the order of events during development (Fig. 4b).

Our study reveals that the inactive state of the Xp and associated epigenetic marks are highly labile during preimplantation development. Their reversal in the ICM may be a reflection of more global reprogramming events occurring at this stage of development (*39*). The reasons for such a dynamic cycle of Xp inactivation, followed by reactivation, followed by random X inactivation in the mouse are unclear but could be due to a combination of evolutionary pressure to silence the Xp early in development, as predicted by the parental genome conflict theory (*40*), together with the efficient reprogramming activity of the ICM.

Finally, in a study investigating X inactivation in cloned mouse embryos (*41*), a GFP transgene carried by a somatic cell–derived in-

active X chromosome, was shown to be reactivated after transfer into an enucleated oocyte, but then became preferentially inactivated in extraembryonic tissues. In light of the results we present here, these findings are consistent with the idea that the presence of a transcribing *Xist* gene, whether paternally inherited or of somatic cell origin, is likely to be the only "imprint" required to trigger the chromatin modifications and epigenetic marks that lead to preferential X inactivation in the cleavage stage embryo.

References and Notes

1. M. F. Lyon, *Nature* **190**, 372 (1961).
2. M. Monk, *Cytogenet. Genome Res.* **99**, 200 (2002).
3. N. Takagi, M. Sasaki, *Nature* **256**, 640 (1975).
4. J. D. West, W. I. Frels, V. M. Chapman, V. E. Papaioannou, *Cell* **12**, 873 (1977).
5. M. F. Lyon, S. Rastan, *Differentiation* **26**, 63 (1984).
6. S. Rastan, *J. Embryol. Exp. Morphol.* **41**, 11 (1982).
7. N. Takagi, O. Sugawara, M. Sasaki, *Chromosoma* **85**, 275 (1982).
8. G. D. Penny, G. F. Kay, S. A. Sheardown, S. Rastan, N, Brockdorff, *Nature* **379**, 131 (1996).
9. Y. Marahrens, B. Panning, J. Dausman, W. Strauss, R. Jaenisch, *Genes Dev.* **11**, 156 (1997).
10. A. Wutz, R. Jaenisch, *Mol. Cell.* **5**, 695 (2000).
11. G. F. Kay, S. C. Barton, M. A. Surani, S. Rastan, *Cell* **77**, 639 (1994).
12. T. B. Nesterova, S. C. Barton, M. A. Surani, N, Brockdorff, *Dev. Biol.* **235**, 343 (2001).
13. M. Zuccotti *et al.*, *Mol. Reprod. Dev.* **61**, 14 (2002).
14. N. Takagi, *Exp. Cell. Res.* **86**, 127 (1974).
15. O. Sugawara, N. Takagi, M. Sasaki, *Cytogenet. Cell Genet.* **39**, 210 (1985).
16. C. J. Epstein, S. Smith, B. Travis, G. Tucker, *Nature* **274**, 500 (1978).
17. P. G. Kratzer, S. M. Gartler, *Nature* **274**, 503 (1978).
18. M. Monk, M. I. Harper, *Nature* **281**, 311 (1979).
19. J. Singer-Sam, V. M. Chapman, J. M. Lebon, A. D. Riggs, *Proc. Natl. Acad. Sci. U.S.A.* **89**, 10469 (1992).
20. K. E. Latham, L. Rambhatla, *Dev. Genet.* **17,** 212 (1995).
21. M. Monk, A. McLaren, *J. Embryol. Exp. Morphol.* **63**, 75 (1981).
22. I. Okamoto, S. S. Tan, N. Takagi, *Development* **127**, 4137 (2000).
23. J. Matsui, Y. Goto, N. Takagi, *Hum. Mol. Genet.* **10**, 1393 (2001).
24. E. Heard *et al.*, *Cell* **107**, 727 (2001).
25. W. Mak *et al.*, *Curr. Biol.* **12**, 1016 (2002).
26. J. Silva *et al.*, *Dev. Cell.* **4**, 481 (2003).
27. K. Plath *et al.*, *Science* **300,** 131 (2003).
28. A. H. Peters *et al.*, *Cell* **107**, 323 (2001).
29. C. Costanzi *et al.*, *Development* **127**, 2283 (2000).
30. J. Chaumeil, I. Okamoto, M. Guggiari, E. Heard, *Cytogenet. Genome Res.* **99**, 75 (2002).
31. J. M. Lebon *et al.*, *Genet. Res.* **65**, 223 (1995).
32. A. K. Hadjantonakis, L. L. Cox, P. P. Tam, A. Nagy, *Genesis* **29**, 133 (2001).
33. M. Patturajan *et al.*, *Mol. Cell. Biol.* **18**, 2406 (1998).
34. J. Chaumeil, E. Heard, in preparation.
35. I. Okamoto, A. P. Otte, C. D. Allis, D. Reinberg, E. Heard, data not shown.
36. J. Rossant, *J. Embryol. Exp. Morphol.* **33**, 991 (1975).
37. See A. P. Otte, T. H. Kwaks, *Curr. Opin. Genet. Dev.* **13**, 448 (2003) for a review.
38. V. E. Papaiioannou, J. D. West, *Genet. Res.* **37**,183 (1981).
39. J. B. Gurdon, J. A. Byrne, S, Simonsson, *Proc. Natl. Acad. Sci. U.S.A.* **100**, 11819 (2003).
40. T. Moore *et al.*, *Dev. Genet.* **17**, 206 (1995).
41. K. Eggan *et al.*, *Science* **290**, 1578 (2000).
42. Materials and methods are available as supporting material on *Science* Online.

43. We thank N. Takagi, V. Colot, and J. Chaumeil for critical reading of the manuscript; J. B. Sibarita for help with 3D microscopy; and S. Yoshida for her encouragement. I.O. was supported by the Japanese Society for the Promotion of Science. This work was funded by the CNRS, the Association pour la Recherche sur le Cancer, and the Fondation pour la Recherche Medicale.

Supporting Online Material
www.sciencemag.org/cgi/content/full/1092727/DC1
Materials and Methods
Figs. S1 to S4
Table S1
References and Notes

20 October 2003; accepted 1 December 2003
Published online 11 December 2003;
10.1126/science.1092727
Include this information when citing this paper.

REPORTS

Extinct Technetium in Silicon Carbide Stardust Grains: Implications for Stellar Nucleosynthesis

Michael R. Savina,[1]* Andrew M. Davis,[2,3] C. Emil Tripa,[1,2] Michael J. Pellin,[1] Roberto Gallino,[4] Roy S. Lewis,[2] Sachiko Amari[5]

The isotopic composition of ruthenium (Ru) in individual presolar silicon carbide (SiC) stardust grains bears the signature of *s*-process nucleosynthesis in asymptotic giant branch stars, plus an anomaly in ^{99}Ru that is explained by the in situ decay of technetium isotope ^{99}Tc in the grains. This finding, coupled with the observation of Tc spectral lines in certain stars, shows that the majority of presolar SiC grains come from low-mass asymptotic giant branch stars, and that the amount of ^{99}Tc produced in such stars is insufficient to have left a detectable ^{99}Ru anomaly in early solar system materials.

Presolar grains, remnants of stars that lived and died before the solar system formed, have much to teach us about stellar evolution and nucleosynthesis. Most of the grains initially present in the protosolar nebula were melted or vaporized when the solar system formed, and were transformed into new mineral phases with isotopic compositions representing an average over all the material present. Some grains, however, accreted into protoplanetary bodies that did not experience substantial heating, survived low-temperature aqueous alteration in those bodies, and are found today in primitive meteorites (*1*, *2*). Each of these presolar grains carries an isotopic record of the initial composition and nuclear processing in its parent star. Silicon carbide grains are the best studied because of their relatively large size (up to several micrometers) and relatively high abundance (up to a few tens of ppm in primitive meteorites) (*3*). Their heavy element concentrations are high enough (up to a few tens of ppm) (*4*) to permit isotopic analysis of trace elements in individual grains. The majority (>90%) of SiC grains were produced in late stellar outflows of low mass (~1.5 to 3 $M_{\odot}$, where $M_{\odot}$ is the mass of the Sun) asymptotic giant branch (AGB) stars (*5*). In AGB stars, elements heavier than Fe are synthesized quiescently by slow neutron capture (the *s*-process), while in massive stars (≥10 $M_{\odot}$) heavy elements are synthesized under explosive conditions by rapid neutron capture (the *r*-process) or by proton capture/photodisintegration reactions (the *p*-process) (*6*). The isotopic compositions of Zr (*7*), Mo (*8*), Sr (*9*), and Ba (*10*) in mainstream SiC grains show the *s*-process signatures predicted by models of nucleosynthesis in carbon-rich low-mass AGB stars from which SiC can condense (*11*).

The pioneering observation of Tc (half-life $T_{1/2} = 2.1 \times 10^5$ years) in the spectra of certain red giants (later recognized as AGB stars) by Merrill more than 50 years ago (*12*) proved that *s*-process nucleosynthesis is ongoing in those stars. Technetium has since been detected in a large proportion of MS, S, and C stars (red giants at various stages of evolution along the AGB) (*13*, *14*). ^{99}Tc lies along the *s*-process path (Fig. 1) and is the only abundant Tc isotope produced in low-mass AGB stars. The

[1]Materials Science Division, Argonne National Laboratory, Argonne, IL 60439, USA. [2]Enrico Fermi Institute, [3]Department of the Geophysical Sciences, University of Chicago, Chicago, IL 60637, USA. [4]Dipartimento di Fisica Generale, Università di Torino and Sezione INFN di Torino, I-10125 Torino, Italy. [5]Laboratory for Space Sciences and Department of Physics, Washington University, St. Louis, MO 63130, USA.

*To whom correspondence should be addressed. E-mail: msavina@anl.gov